X-rays from relativistic electrons crossing a multilayer nanostructure

N.N. Nasonov [a,*], V.V. Kaplin [b], S.R. Uglov [b], V.N. Zabaev [b], M.A. Piestrup [c], C.K. Gary [c]

[a] *Laboratory of Radiation Physics, Belgorod State University, 14 Studencheskaya street, Belgorod 308007, Russia*
[b] *Nuclear Physics Institute, Tomsk Polytechnic University, P.O. Box 25, Tomsk 634050, Russia*
[c] *Adelphi Technology Inc., 981-B Industrial Road, San Carlos, CA 94070, USA*

Abstract

The results of theoretical and experimental studies of X-ray emission from relativistic electrons crossing periodic nanostructures are presented in this work. Simple formulae describing the characteristics of the total emission from either thin-non-absorbing or thick-absorbing multilayers are derived, accounting for both diffracted-transition and parametric-radiation mechanisms. The measured vertical spatial distributions and orientation dependencies (rocking curves) of the spectra of this type of radiation are presented. Good agreement between theory and experimental results is shown. The results demonstrate the possibility of a tunable quasimonochromatic X-ray source whose efficiency can be larger than that of other novel X-ray sources.

Keywords: X-ray emission; Multilayer nanostructure; Parametric X-rays; Diffracted transition radiation

1. Introduction

A number of novel sources based on transition-, channeling- and parametric-emission mechanisms have been considered as possible candidates for industrial, medical and scientific applications [1–4]. However, their output brightness is marginal for most applications even if very high current electron beams are used [5]. The efficiency of these novel sources must be increased for their use to be practical. This has stimulated the search for more efficient mechanisms of X-ray generation in other types of periodic structures which might give

* Corresponding author. Tel.: +7 22 341477; fax: +7 22 341692.
E-mail address: nnn@bsu.edu.ru (N.N. Nasonov).

monochromatic and low-divergent photon beams of high brightness.

Previously, we presented experimental results of X-ray production from relativistic electrons traversing periodic multilayer nanostructures or X-ray mirrors [6]. The experiment was carried out at the Tomsk "Sirius" synchrotron using a 500-MeV electron beam. A multilayer consisting of pairs of W and B_4C layers $N=300$ and period $T=12.36$ Å was used as a radiator for the generation of 15 keV photons. The X-rays were emitting at the Bragg angle $=1.9°$ with respect to the multilayer surface and at the angle 3.8° with respect to the electron-beam direction. The spatial distribution and orientation dependence of the yield were measured. The experiment showed that the emission mechanism was highly efficient for X-ray production for a broad range of photon energies.

The present work is devoted to further theoretical and experimental studies of the multilayer emission mechanism. Experimentally, we have studied multilayers with both cluster-graded and uniform periods. We present a simple description of the emission process for the given experimental parameters and for the maximum emission from a multilayer for two different electron energy ranges. Fundamental tenets of such a model have been presented recently in our work [7]. A detailed theoretical description of emission characteristics is given here.

Multilayer structures have been considered for the most part as radiators for the production of resonant transition–radiation [8–11]. However, other emission mechanisms are possible for the same structure [7]. Indeed, if the structure is placed in the Bragg condition, the X-rays can be scattered out and two processes, diffracted transition radiation (DTR) and parametric X-ray radiation (PXR), can occur as it does in crystalline targets [3,4,12–16].

Since the period of the multilayer can be comparable to the wave length of emitted photons, we go beyond the scope of the Wentzel–Kramers–Brillouin approximation normally used in such analyses [8]. Other methods have been used to describe the emission processes in multilayer structures [17–24]. In our opinion, the best approach to such a task uses X-ray dynamic-diffraction theory [25]. Previously, this approach, and its simple limit known as kinematic-scattering theory or perturbation theory, were used to describe PXR and DTR processes in crystalline targets [12,13,26]. The important difference between these processes in a crystal and a multilayer is the multilayer's emission mechanism and its possible increased yield. For the case of a multilayer the number of the target's electrons making a coherent contribution to the formation of PXR and DTR (the difference between numbers of electrons in two alternate layers) is much larger than that of a crystal (the number of electrons in a single atomic plane) and, therefore, the total-emission yield from a multilayer can exceed the yield from the crystal.

As in [17,24] we use the dynamic-diffraction theory to analyze the emission from relativistic electrons crossing a multilayer. The main difference between our approach and that normally used consists of the separation of the total-emission amplitude into PXR and DTR amplitudes (see [27,28]). Such an approach allows us to elucidate in more detail the relation between PXR and DTR relative contributions to the formation of the total-emission yield. Among with other issues, this is of importance because the DTR contribution was not considered in [17,24].

The paper is organized as follows. In Section 2 the analytical description of X-ray emission from relativistic electrons crossing a multilayer is developed. The contributions of PXR and DTR are considered separately as well as the interference between them. Section 3 is devoted to the discussion of experiments measuring the X-ray emission from multilayers having the uniform and cluster-graded periods. We compare the obtained theoretical and experimental results in Section 4. Conclusions are given in Section 5.

2. Theoretical description

2.1. General expressions

We will first determine the electromagnetic field emitted from a relativistic electron moving in a

medium with periodic-dielectric susceptibility $\chi(\omega,\mathbf{r})=\chi_0(\omega)+\sum'_{\mathbf{g}}\chi_{\mathbf{g}}(\omega)e^{i\mathbf{gr}}$. For the case of a one-dimensional structure consisting of alternative layers of thicknesses a and b, and susceptibilities $\chi_a(\omega)$ and $\chi_b(\omega)$, respectively, the quantities $\chi_0(\omega)$ and $\chi_{\mathbf{g}}(\omega)$ are determined by the expressions

$$\chi_0(\omega)=\frac{a}{T}\chi_a+\frac{b}{T}\chi_b,$$
$$\chi_{\mathbf{g}}(\omega)=\frac{1-e^{iqa}}{igT}(\chi_a-\chi_b), \tag{1}$$

where $T=a+b$ is the period of multilayered structure, $\mathbf{g}=\mathbf{e}_x g$, $g\equiv g_n=\frac{2\pi}{T}n$, $n=0,\pm1,\pm2,\ldots$, $\mathbf{e}_x$ is the normal to the surface of a layer (see Fig. 1). The Fourier-transform of the electric field

$$\mathbf{E}_{\omega\mathbf{k}}=(2\pi)^{-4}\int dt\,d^3r e^{-i\mathbf{kr}+i\omega t}\mathbf{E}(\mathbf{r},t)$$

is determined by Maxwell's equation:

$$(k^2-\omega^2)\mathbf{E}_{\omega\mathbf{k}}-\mathbf{k}(\mathbf{kE}_{\omega\mathbf{k}})-\omega^2\chi_0\mathbf{E}_{\omega\mathbf{k}}$$
$$-\omega^2\sum'_{\mathbf{g}}\chi_{-\mathbf{g}}\mathbf{E}_{\omega\mathbf{k}+\mathbf{g}}=\frac{i\omega e}{2\pi^2}\mathbf{v}\delta(\omega-\mathbf{kv}), \tag{2}$$

where $\mathbf{v}$ is the emitting particle velocity. Since $\chi_0,\chi_{\mathbf{g}}\ll 1$ for X-rays, the solution of (2) can be obtained from the two-wave approximation of the dynamic-diffraction theory [25]. Taking into account that the field components $\mathbf{E}_{\omega\mathbf{k}}$ and $\mathbf{E}_{\omega\mathbf{k}+\mathbf{g}}$ are approximately transverse to the vectors $\mathbf{k}$ and $\mathbf{k}+\mathbf{g}$, respectively [29], we reduce (2) to two well-known equations:

$$(k^2-\omega^2-\omega^2\chi_0)E_{\lambda 0}-\omega^2\chi_{-\mathbf{g}}\alpha_\lambda E_{\lambda\mathbf{g}}$$
$$=\frac{i\omega e}{2\pi^2}\mathbf{e}_{\lambda 0}\mathbf{v}\delta(\omega-\mathbf{kv}), \tag{3a}$$

$$((\mathbf{k}+\mathbf{g})^2-\omega^2-\omega^2\chi_0)E_{\lambda\mathbf{g}}-\omega^2\chi_{\mathbf{g}}\alpha_\lambda E_{\lambda 0}=\mathbf{0}, \tag{3b}$$

where new quantities have been defined by the expressions

$$\mathbf{E}_{\omega\mathbf{k}}=\sum_{\lambda=1}^{2}\mathbf{e}_{\lambda 0}E_{\lambda 0},\quad \mathbf{E}_{\omega\mathbf{k}+\mathbf{g}}=\sum_{\lambda=1}^{2}\mathbf{e}_{\lambda\mathbf{g}}E_{\lambda\mathbf{g}},$$
$$\mathbf{e}_{10}=\mathbf{e}_{1\mathbf{g}}=\frac{[\mathbf{k}_\parallel,\mathbf{e}_x]}{k_\parallel},\quad \mathbf{e}_{20}=\frac{[\mathbf{k},\mathbf{e}_{10}]}{k},\quad \mathbf{e}_{2\mathbf{g}}=\frac{[\mathbf{k}+\mathbf{g},\mathbf{e}_{10}]}{|\mathbf{k}+\mathbf{g}|},$$
$$\alpha_1=1,\quad \alpha_2=\mathbf{k}(\mathbf{k}+\mathbf{g})/k|\mathbf{k}+\mathbf{g}|,$$
$$\mathbf{k}=\mathbf{e}_x k_x+\mathbf{k}_\parallel,\quad \mathbf{e}_x\mathbf{k}_\parallel=0. \tag{4}$$

Eqs. (3) describe the electromagnetic field inside the multilayer. The corresponding wave-equations for field components $E^{\mathrm{V}}_{\lambda 0}$ and $E^{\mathrm{V}}_{\lambda\mathbf{g}}$ in the vacuum outside the target follow from (3) in the limit $\chi_0=\chi_{\mathbf{g}}=0$. Since only the Bragg geometry can be realized for a multilayer (Laue geometry for a multilayer is mechanically impossible at this time), it is sufficient to determine the components $E^{\mathrm{V}}_{\lambda 0}$ and $E^{\mathrm{V}}_{\lambda\mathbf{g}}$ in the vacuum in front of the multilayer (region $x>0$ in Fig. 1). Using the general expressions for the field components $E_{\lambda 0,\mathbf{g}}$ and $E^{\mathrm{V}}_{\lambda 0,\mathbf{g}}$ following from the corresponding wave equations (the solutions

$$E^{\mathrm{V}}_{\lambda\mathbf{g}}=a_{\lambda\mathbf{k}_\parallel}\delta(k_{gx}-p),\quad p=\sqrt{\omega^2-k_\parallel^2},$$
$$k_{gx}=k_x+g, \tag{5}$$

describing the emission field in a vacuum) and the ordinary boundary conditions for electromagnetic fields on front- and back-surfaces of the multilayer

$$\int dk_x(E_{\lambda 0}-E^{\mathrm{V}}_{\lambda 0})=\int dk_x e^{-ik_x L}E_{\lambda\mathbf{g}}$$
$$=\int dk_x(E_{\lambda g}-E^{\mathrm{V}}_{\lambda g})=0, \tag{6}$$

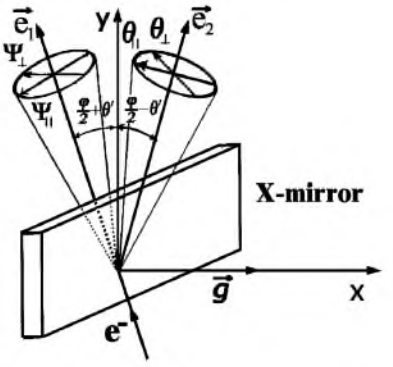

Fig. 1. The geometry of the emission process. A multilayer mirror is positioned at the Bragg condition in an electron beam to generate X-rays. $\mathbf{g}$ is the reciprocal lattice vector, $\mathbf{e}_1$ is the electron-beam axis, $\mathbf{e}_2$ is the photon collimator axis, φ is the emission angle, θ' is the orientational angle, which may be changed by the goniometer, $\Theta_\parallel$ and $\Psi_\parallel$ are the components of the angular variables $\mathbf{\Theta}$ and $\mathbf{\Psi}$ parallel to the plane determined by the vectors $\mathbf{e}_1$ and $\mathbf{e}_2$, $\Theta_\perp$ and $\Psi_\perp$ are the components perpendicular to such a plane.

we can determine the coefficient $a_{\lambda\mathbf{k}_\parallel}$. Since solving this equation is the standard task of dynamic-diffraction theory, we present the final result only

$$a_{\lambda\mathbf{k}_\parallel} = \frac{\mathrm{i}\omega^3 e\chi_{\mathbf{g}}\alpha_\lambda \mathbf{e}_{\lambda 0}\mathbf{v}}{8\pi^2 p^2 |v_x|}\frac{A}{B},$$

$$A = \left(\frac{1}{\Delta_0} - \frac{1}{\Delta_1 - \xi_1}\right)\left(1 - \mathrm{e}^{-\mathrm{i}(\Delta_1 - \xi_1)L}\right) - \left(\frac{1}{\Delta_0} - \frac{1}{\Delta_1 - \xi_2}\right)\left(1 - \mathrm{e}^{-\mathrm{i}(\Delta_1 - \xi_2)L}\right),$$

$$B = \xi_2 \mathrm{e}^{-\mathrm{i}(\Delta_1 - \xi_2)L} - \xi_1 \mathrm{e}^{-\mathrm{i}(\Delta_2 - \xi_1)L}, \tag{7}$$

where

$$\Delta_0 = \frac{1}{|v_x|}(\omega - \mathbf{k}_\parallel \mathbf{v}_\parallel - p|v_x|), \qquad \Delta_1 = \Delta_0 - \frac{\omega^2}{2p}\chi_0,$$

$$\xi_{1,2} = \frac{1}{2}\left(\Delta' \pm \sqrt{\Delta'^2 - \frac{\omega^4}{p^2}\chi_{\mathbf{g}}\chi_{-\mathbf{g}}\alpha_\lambda^2}\right),$$

$$\Delta' = \Delta - \frac{\omega^2}{p}\chi_0, \quad \Delta = g\left(\frac{g}{2p} - 1\right). \tag{8}$$

An influence of the dynamic-diffraction effects on the emission properties is described in the general solution (7) by the variables Δ and $\xi_{1,2}$ (this influence is important if $\Delta^2 \leqslant \frac{\omega^4}{p^2}\chi_{\mathbf{g}}\chi_{-\mathbf{g}}\alpha_\lambda^2$). The quantities $\xi_{1,2}$ determine two different solutions to the dispersion equation $k_{gx} = k_{gx}^{(1,2)} \equiv p + \frac{\omega^2}{2p}\chi_0 + \xi_{1,2}$, and Δ is the so-called resonance defect.

To determine the emission amplitude A_λ we calculate the Fourier-integral

$$E_\lambda^{\mathrm{Rad}} = \int \mathrm{d}^3 k_g \mathrm{e}^{\mathrm{i}\mathbf{k}_\mathbf{g}\mathbf{n}r} E_{\lambda\mathbf{g}}^{\mathrm{V}}, \tag{9}$$

where $\mathbf{n}$ is the unit vector in the direction of emitted photon propagation. The field E_λ^{Rad} in the wave-zone is calculated by the stationary-phase method:

$$E_\lambda^{\mathrm{Rad}} = A_\lambda \frac{\mathrm{e}^{\mathrm{i}\omega r}}{r}, \quad A_\lambda = -2\pi\mathrm{i}\omega n_x a_{\lambda\omega\mathbf{n}_\parallel}, \tag{10}$$

where $\mathbf{n} = \mathbf{n}_\parallel + \mathbf{e}_x n_x$, $\mathbf{e}_x \mathbf{n}_\parallel = 0$.

The expressions (7), (8) and (10) give a detailed description of the emission amplitude A_λ. To simplify this result we define the angular variables $\boldsymbol{\Theta}$ and $\boldsymbol{\Psi}$ in accordance with the formulae

$$\mathbf{v} = \mathbf{e}_1\left(1 - \frac{1}{2}\gamma^{-2} - \frac{1}{2}\Psi^2\right) + \boldsymbol{\Psi}, \quad \mathbf{e}_1\boldsymbol{\Psi} = 0, \tag{11a}$$

$$\mathbf{n} = \mathbf{e}_2\left(1 - \frac{1}{2}\Theta^2\right) + \boldsymbol{\Theta}, \quad \mathbf{e}_2\boldsymbol{\Theta} = 0, \quad \mathbf{e}_1\mathbf{e}_2 = \cos\varphi, \tag{11b}$$

where γ is the Lorentz-factor of an emitting particle. The components of the angular variables $\boldsymbol{\Psi} = \boldsymbol{\Psi}_\parallel + \boldsymbol{\Psi}_\perp$, $\boldsymbol{\Psi}_\perp\boldsymbol{\Psi}_\parallel = 0$ and $\boldsymbol{\Theta} = \boldsymbol{\Theta}_\parallel + \boldsymbol{\Theta}_\perp$, $\boldsymbol{\Theta}_\perp\boldsymbol{\Theta}_\parallel = 0$ are shown in Fig. 1. In addition to this it is very convenient to separate the total amplitude A_λ into two components: a PXR emission amplitude A_λ^{PXR} and a DTR emission amplitude A_λ^{DTR}.

The final expression for the emission amplitude A_λ has the form

$$A_\lambda = A_\lambda^{\mathrm{PXR}} + A_\lambda^{\mathrm{DTR}}, \tag{12a}$$

$$A_\lambda^{\mathrm{PXR}} = \frac{e\omega^2\chi_{\mathbf{g}}\alpha_\lambda}{4\pi\sin^2(\varphi/2)}\frac{\mathbf{e}_{\lambda 0}\mathbf{v}}{\xi_2\mathrm{e}^{-\mathrm{i}(\Delta_1 - \xi_2)L} - \xi_1\mathrm{e}^{-\mathrm{i}(\Delta_1 - \xi_1)L}} \times \left[\frac{\xi_2}{\Delta_1}\frac{1 - \mathrm{e}^{-\mathrm{i}(\Delta_1 - \xi_2)L}}{\Delta_1 - \xi_2} - \frac{\xi_1}{\Delta_1}\frac{1 - \mathrm{e}^{-\mathrm{i}(\Delta_1 - \xi_1)L}}{\Delta_1 - \xi_1}\right], \tag{12b}$$

$$A_\lambda^{\mathrm{DTR}} = \frac{e\omega^2\chi_{\mathbf{g}}\alpha_\lambda}{4\pi\sin^2(\varphi/2)}\mathbf{e}_{\lambda 0}\mathbf{v}\left[\frac{1}{\Delta_0} - \frac{1}{\Delta_1}\right]\frac{\mathrm{e}^{\mathrm{i}\xi_2 L} - \mathrm{e}^{\mathrm{i}\xi_1 L}}{\xi_2\mathrm{e}^{\mathrm{i}\xi_2 L} - \xi_1\mathrm{e}^{\mathrm{i}\xi_1 L}}, \tag{12c}$$

where the quantities Δ_0, Δ_1 and Δ' appearing in Eq. (12) and defined above by (8) can be presented as

$$\Delta_0 = \frac{\omega}{2\sin(\varphi/2)}[\gamma^{-2} + (\Theta_\perp - \Psi_\perp)^2 + (2\theta' + \Theta_\parallel + \Psi_\parallel)^2],$$

$$\Delta_1 = \Delta_0 - \frac{\omega}{2\sin(\varphi/2)}\chi_0,$$

$$\Delta' = g\left[\frac{\omega'_{\mathrm{B}}}{\omega} - 1 - \frac{\chi_0}{2\sin^2(\varphi/2)}\right] \approx g\left(\frac{\omega'_{\mathrm{B}}}{\omega} - 1\right) \equiv \Delta. \tag{13}$$

The important quantity ω'_{B} in (13),

$$\omega'_{\mathrm{B}} = \omega_{\mathrm{B}}\left[1 + (\theta' + \Theta_\parallel)\cot\left(\frac{\varphi}{2}\right)\right],$$

$$\omega_{\mathrm{B}} = \frac{g}{2\sin(\varphi/2)}, \tag{14}$$

where ω_B is the Bragg frequency. In the vicinity of where the emission is concentrated ω'_B describes the dependence of characteristic energy of the emission on both the orientation angle θ' (this angle is subject to wide variations by the goniometer in which the multilayer is installed) and the observation angle $\Theta_\parallel$.

The quantities $\Delta_0 L$ and $\Delta_1 L$ are the ratios of an emitting electron's path in the multilayer $L/\sin(\varphi/2)$ to the emission formation length in (1) a vacuum and in (2) a medium with an average dielectric susceptibility χ_0, respectively.

The result (12) allows us to (1) compare the efficiencies of multilayer and crystalline radiators, (2) estimate the relative DTR and PXR contributions to total-emission yield for various parameter ranges and (3) compare theory with obtained experimental results.

2.2. DTR contribution

Let us consider first the DTR contribution from a thin target with a thickness smaller than the photoabsorption length. The expression for the DTR spectral–angular distribution follows from (12c),

$$\omega\frac{dN_\lambda^{DTR}}{d\omega\, d^2\Theta} = \frac{e^2}{\pi^2}\left\langle \Omega_\lambda^2\left(\frac{1}{\gamma^{-2}+\Omega^2}-\frac{1}{\gamma^{-2}-\chi_0+\Omega^2}\right)^2\right\rangle \times R_\lambda^{DTR}(t_\lambda,\tau_\lambda), \tag{15a}$$

$$R_\lambda^{DTR} = \frac{|\sin(t_\lambda\sqrt{\tau_\lambda^2-1})|^2}{|\tau_\lambda^2-1|+|\sin(t_\lambda\sqrt{\tau_\lambda^2-1})|^2}, \tag{15b}$$

where $\Omega_1=\Theta_\perp-\Psi_\perp$, $\Omega_2=2\theta'+\Theta_\parallel+\Psi_\parallel$, $\Omega^2=\Omega_1^2+\Omega_2^2$, the brackets $\langle\rangle$represent the averaging over the angles $\Psi_\perp$ and $\Psi_\parallel$ that describe the angular spread in the beam of emitting electrons. The coefficient t_λ and the function $\tau_\lambda(\omega)$ are defined by

$$t_\lambda = \frac{\omega|\chi_{\mathbf{g}}|L\alpha_\lambda}{2\sin(\varphi/2)},$$
$$\tau_\lambda(\omega) = \frac{2\sin^2(\varphi/2)}{|\chi_{\mathbf{g}}|\alpha_\lambda}\left(1-\frac{\omega}{\omega'_B}\right). \tag{16}$$

The physical meaning of these quantities is as follows: t_λ is a half of the ratio of electron path in the target $L/\sin(\varphi/2)$ to the extinction length $1/\omega|\chi_{\mathbf{g}}|\alpha_\lambda$. The rapidly-changing variable $\tau_\lambda(\omega)$ is the ratio of the resonance defect Δ to the width of Bragg resonance $\omega|\chi_{\mathbf{g}}|\alpha_\lambda/\sin(\varphi/2)$.

The result (15) shows that DTR arises due to dynamic scattering of the transition radiation emitted by a relativistic electron from the front-surface of the multilayer. The front-half of (15a) describes single-interface transition radiation [1], while R_λ^{DTR} in (15b) is a reflection coefficient. From (15b) the function R_λ^{DTR} decreases proportional to τ_λ^{-2} outside the narrow frequency range close to the Bragg frequency ω_B, where $|\tau_\lambda(\omega)|<1$ and anomalous dispersion for X-rays is realized. As a consequence the DTR spectral width has a value of about

$$\Delta\omega/\omega \approx \frac{|\chi_{\mathbf{g}}|\alpha_\lambda}{2\sin^2(\varphi/2)} \approx \frac{2\omega_{\mathbf{g}}^2\alpha_\lambda}{g^2} \equiv \frac{2\alpha_\lambda}{g^2}\frac{\sin\left(\pi\frac{a}{T}\right)}{\pi}|\omega_a^2-\omega_b^2| \ll 1, \tag{17}$$

where the quantity $\omega_{\mathbf{g}}^2$ follows from (1) and the simplest approximation for the dielectric susceptibilities $\chi_{a,b}=-\omega_{a,b}^2/\omega^2$, so that

$$\chi_0 = -\omega_p^2/\omega^2, \quad \omega_p^2 = \frac{a}{T}\omega_a^2+\frac{b}{T}\omega_b^2,$$
$$|\chi_{\mathbf{g}}| = \omega_{\mathbf{g}}^2/\omega^2. \tag{18}$$

The condition (17) allows to consider the frequency ω in (15) as constant except the "fast variable" $\tau_\lambda(\omega)$. Setting $\omega\approx\omega_B$ we can determine the range of electron energies, where DTR contribution can be large,

$$\gamma > \gamma_* = \frac{\omega_B}{\omega_p} = \frac{\pi}{\omega_p T\sin(\varphi/2)}. \tag{19}$$

Indeed, DTR yield is proportional to $\gamma^4/\gamma_*^4 \ll 1$ if $\gamma<\gamma_*$ in accordance with (15a) and general properties of the transition radiation.

The important coefficient t_λ in (15b) determines the efficiency of transition radiation reflection by the multilayer. Integrating (15) over ω one can obtain the following expression for the DTR angular distribution:

$$\frac{dN_\lambda^{DTR}}{d^2\Theta} = \frac{2e^2\omega_{\mathbf{g}}^2\alpha_\lambda}{\pi g^2} \times \tanh(t_\lambda)\left\langle \Omega_\lambda^2\left(\frac{1}{\gamma^{-2}+\Omega^2} - \frac{1}{\gamma^{-2}+\frac{\omega_0^2}{\omega^2}+\Omega^2}\right)^2\right\rangle. \quad (20)$$

When integrating over ω the transformation of variables $d\omega = (\frac{d\tau_\lambda(\omega)}{d\omega})^{-1}d\tau_\lambda$ has been used.

The function $\tanh(\tau_\lambda)$ in (20) illustrates the effect of DTR yield saturation as a function of the multilayer thickness L or the number of periods in multilayer $M = L/T$. The optimum number of periods M_{opt}^{DTR} following from (20) is given by

$$M_{opt}^{DTR} \approx \frac{g^2}{\pi\omega_{\mathbf{g}}^2\alpha_\lambda} = \left(\frac{2\pi}{T}\right)^2 \frac{1}{\sin(\pi\frac{a}{T})|\omega_a^2 - \omega_b^2|}. \quad (21)$$

In accordance with (21) M_{opt}^{DTR} decreases with an increase in multilayer period T.

As it follows from (20), the DTR angular density is proportional to the square of the period T. Since this period is larger than that of a crystal's, DTR brightness from multilayer can be much greater than that from a crystal. For example, $dN^{DTR}/d^2\Theta \approx 6$ photons/electron·str. under condition of $\omega_a \approx 80$ eV (W layer), $\omega_a \gg \omega_b$, $T \approx 20$ Å, $\gamma \approx 10^3$, $a = T/2$. This is two orders of magnitude brighter than that from a W crystal.

The formula for DTR photon-number follows from (20) after integrating over $\boldsymbol{\Theta}$, and has a simple form of

$$N_\lambda^{DTR} = \frac{e^2\omega_{\mathbf{g}}^2\alpha_\lambda}{2g^2}\tanh(t_\lambda) \times \left[\left(1+2\frac{\gamma_*^2}{\gamma^2}\right)\ln\left(\frac{(1+\gamma^2\Theta_d^2)(1+\gamma^2/\gamma_*^2)}{1+\gamma^2\Theta_d^2+\gamma^2/\gamma_*^2}\right) - \frac{\gamma^2\Theta_d^2}{1+\gamma^2\Theta_d^2} - \frac{\gamma^2\Theta_d^2}{1+\gamma^2\Theta_d^2+\gamma^2/\gamma_*^2}\right], \quad (22)$$

where Θ_d is the photon collimator angular size, which is assumed to be large relative to the multiple scattering angle.

Since the target dielectric characteristics are presented in (22) by the quantities $\omega_{\mathbf{g}}^2$ and γ_* only, one can use the result to describe arbitrary targets with periodic dielectric susceptibilities including crystals. Let us compare crystalline and multilayer DTR radiators. Assuming the Bragg frequency $\omega_{\mathbf{B}}$ to be far from absorption edges for the crystal material, we introduce the quantity $\omega_{\mathbf{g}}^2$ so that $|\chi_{\mathbf{g}}| = \omega_{\mathbf{g}(cr)}^2/\omega^2$ ($\omega_{\mathbf{g}(cr)}^2 \approx \omega_{p\,cr}^2(F(g)/Z)(|S(\mathbf{g})|/N_c)e^{-\frac{1}{2}g^2u_T^2}$, where $\omega_{p(cr)}$ is the plasma frequency of the crystal, $F(g)$ is the atomic-form factor, Z is the number of electrons in an atom, $S(\mathbf{g})$ is the structure factor of a crystalline elementary cell, containing N_c atoms, u_T is the mean-square amplitude of atom thermal vibrations). The ratio of DTR yield from a crystal to that from a multilayer is

$$\frac{N_{\lambda(cr)}^{DTR}}{N_{\lambda(mul)}^{DTR}} \approx \frac{\omega_{\mathbf{g}(cr)}^2}{\omega_{\mathbf{g}(mul)}^2}\frac{T_{(cr)}^2}{T_{(mul)}^2} = \frac{\Delta\omega_{(cr)}^{DTR}}{\Delta\omega_{(mul)}^{DTR}} \quad (23)$$

following from (22) on condition of thick targets ($t_\lambda > 2$). Since the quantities $\omega_{\mathbf{g}(cr)}^2$ and $\omega_{\mathbf{g}(mul)}^2$ are comparable (see above definitions), (23) predicts a higher efficiency of a multilayer as a DTR radiator relative to a crystalline one, since $T_{(mul)}$ exceeds $T_{(cr)}$. On the other hand (23) shows that the spectral width of DTR flux emitted from the crystalline radiator is smaller than that from the multilayer.

2.3. PXR contribution. Influence of an interference between PXR and DTR

We will now use the general formula (12b) to analyze the contribution of PXR to total-emission yield. From (12b) the PXR amplitude consists of two terms corresponding to two branches of possible electromagnetic waves in a periodical target. The magnitudes of the contributions of these terms are the similar for the case of thin-multilayer thickness L (i.e. $t_\lambda < 1$); but the PXR yield is small in this case. In the more important case of a thick multilayer $t_\lambda \gg 1$, the main contribution to PXR yield has only one term containing the quantity ξ, because the denominator of this term can be 0. For this case we obtain

$$\omega\frac{dN_\lambda^{PXR}}{d\omega\,d^2\Theta} = \frac{e^2}{\pi^2}\left\langle \frac{\Omega_\lambda^2}{(\gamma^{-2}+\gamma_*^{-2}+\Omega^2)^2}R_\lambda^{PXR}\right\rangle, \quad (24a)$$

$$R_\lambda^{\mathrm{PXR}} = \frac{(\tau_\lambda + \sqrt{\tau_\lambda^2 - 1})^2}{\tau_\lambda^2 - 1 + \sin^2(t_\lambda \sqrt{\tau_\lambda^2 - 1})} \times \frac{\sin^2[\frac{1}{2} t_\lambda (\tau_\lambda + \sqrt{\tau_\lambda^2 - 1} - (\gamma^{-2} + \gamma_*^{-2} + \Omega^2)/|\chi_{\mathrm{g}}|\alpha_\lambda)]}{[\tau_\lambda + \sqrt{\tau_\lambda^2 - 1} - (\gamma^{-2} + \gamma_*^{-2} + \Omega^2)/|\chi_{\mathrm{g}}|\alpha_\lambda]^2}. \tag{24b}$$

The factor $(e^2/\pi^2)\Omega_\lambda^2/(\gamma^{-2} + \gamma_*^{-2} + \Omega^2)^2$ in (24a) describes the distribution of the coulomb field of a relativistic particle moving in a medium with the dielectric permeability $\epsilon(\omega) = 1 + \chi_0(\omega)$. This field is screened by the density effect appearing due to the polarization of medium electrons by the electromagnetic field. The coefficient R_λ^{PXR} describes the coherent scattering of the coulomb field by the multilayer structure.

When $t_\lambda \gg 1$ the function R_λ^{PXR} has a sharp maximum in the vicinity of $\tau_\lambda = \tau_{*\lambda}$,

$$\tau_{*\lambda} = 1 + \frac{(\gamma^{-2} + \gamma_*^{-2} + \Omega^2 - |\chi_{\mathrm{g}}|\alpha_\lambda)^2}{2(\gamma^{-2} + \gamma_*^{-2} + \Omega^2)|\chi_{\mathrm{g}}|\alpha_\lambda} > 1. \tag{25}$$

In accordance with (25), the PXR peak is outside the range of anomalous dispersion, where $|\tau_\lambda| < 1$ and DTR dominates. It should be noted that the large change of the rapidly-changing variable $\tau_\lambda(\omega)$ defined by (16), corresponds to a small change of ω. Therefore the difference between DTR and PXR emission frequencies is very small (about 10 eV) and, therefore, difficult to measure experimentally.

The distribution (24) can be integrated over ω for the practical case $t_\lambda \gg 1$ by using the approximation $\sin^2(tx)/x^2 \to \pi t \delta(x)$. The result of integration,

$$\frac{N_\lambda^{\mathrm{PXR}}}{\mathrm{d}^2\Theta} = \frac{2e^2\omega_{\mathrm{g}}^2\alpha_\lambda}{\pi g^2} t_\lambda \left\langle \frac{\Omega_\lambda^2}{(\gamma^{-2} + \gamma_*^{-2} + \Omega^2)^2 - |\chi_{\mathrm{g}}|^2\alpha_\lambda^2} \times \left[1 + \frac{4(\gamma^{-2} + \gamma_*^{-2} + \Omega^2)^2 |\chi_{\mathrm{g}}|^2 \alpha_\lambda^2}{((\gamma^{-2} + \gamma_*^{-2} + \Omega^2)^2 - |\chi_{\mathrm{g}}|^2\alpha_\lambda^2)^2} \times \sin^2\left(t_\lambda \frac{(\gamma^{-2} + \gamma_*^{-2} + \Omega^2)^2 - |\chi_{\mathrm{g}}|^2\alpha_\lambda^2}{2(\gamma^{-2} + \gamma_*^{-2} + \Omega^2)|\chi_{\mathrm{g}}|\alpha_\lambda}\right)\right]^{-1} \right\rangle, \tag{26}$$

allows us not only to compare the efficiencies of PXR radiators using either a crystal or a multilayer, but also to estimate an influence of dynamic-diffraction effects on PXR properties as well.

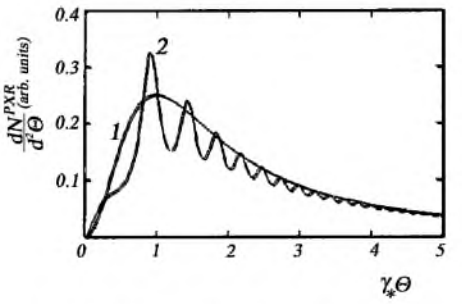

Fig. 2. $\mathrm{d}N^{\mathrm{PXR}}/\mathrm{d}^2\Theta$ plotted as a function of the angular variable $\gamma_*\Theta$ ($\gamma \gg \gamma_*$). This figure shows the influence of dynamic diffraction on the PXR angular distribution as given by (26) for $t_\lambda = 4$ and for two cases of $\omega_{\mathrm{g}}^2/\omega_{\mathrm{p}}^2 = 0$; 0.9 (curves 1 and 2, respectively).

The formula (26) reduces to well the known kinematic limit of the PXR angular distribution, if $\gamma < \gamma_*$. If $\gamma > \gamma_*$, then the difference between kinematic and dynamic results can be important provided $\gamma_*|\chi_{\mathrm{g}}| = \omega_{\mathrm{g}}^2/\omega_{\mathrm{p}}^2 \approx 1$. In this case the strong oscillations appear in the PXR angular distribution, as is illustrated by the curves presented in Fig. 2.

Let us compare DTR and PXR angular densities. The ratio

$$\frac{\mathrm{d}N_\lambda^{\mathrm{DTR}}}{\mathrm{d}^2\Theta} \Big/ \frac{\mathrm{d}N_\lambda^{\mathrm{PXR}}}{\mathrm{d}^2\Theta} \approx \frac{\tanh(t_\lambda)}{t_\lambda} \frac{\gamma^4/\gamma_*^4}{(1 + \gamma^2\Omega^2)^2}, \tag{27}$$

following from (20) and (26), shows that DTR angular density for high enough emitting electron energies $\gamma \gg \gamma_*$ dominates in the region of small observation angles $\Theta \leqslant \gamma^{-1}$, even though the DTR yield is saturated ($t_\lambda \gg 1$).

As noted above, the condition $\omega_{\mathrm{g}}^2/\omega_{\mathrm{p}}^2 \approx 1$ must be fulfilled for the dynamic-diffraction effects in PXR to happen. In accordance with (17) such a condition can be fulfilled with the proviso that $\omega_a^2 \gg \omega_b^2$ and $a \ll T$. On the other hand, the relation $a = \frac{1}{2}T$ is best suited to X-ray producing by a multilayer because DTR and PXR yields are proportional to $\sin(\pi\frac{a}{T})$ and $\sin^2(\pi\frac{a}{T})$, respectively in accordance with (20) and (26). As this takes place $\omega_{\mathrm{g}}^2/\omega_{\mathrm{p}}^2 < 2/\pi$ and therefore an influence of dynamic-diffraction effects is small for the most

practical case. With this conclusion the PXR yield follows from (26) in the form

$$N_\lambda^{\mathrm{PXR}} = \frac{e^2\omega_{\mathbf{g}}^2\alpha_\lambda}{g^2} t_\lambda \times \left[\ln\left(1+\frac{\gamma^2\Theta_d^2}{1+\gamma^2/\gamma_*^2}\right) - \frac{\gamma^2\Theta_d^2}{1+\gamma^2\Theta_d^2+\gamma^2/\gamma_*^2}\right]. \tag{28}$$

The result (28) allows us to compare DTR and PXR yields from a multilayer to elucidate the possibilities of the multilayer as a radiator. On condition $\gamma \gg \gamma_*$, $\gamma_*^2\Theta_d^2 \gg 1$ under consideration, the ratio

$$\frac{N_\lambda^{\mathrm{DTR}}}{N_\lambda^{\mathrm{PXR}}} \approx \frac{\tanh(t_\lambda)}{2t_\lambda}\frac{\ln(\gamma/\gamma_*)}{\ln(\gamma_*\Theta_d)}, \tag{29}$$

following from (22) and (28), shows that the total yield of weakly collimated emission from the thick multilayer ($t_\lambda \gg 1$) is determined in the main by the PXR emission mechanism in contrast with that for strongly collimated emission (see (27)).

Since the PXR yield is proportional to the target thickness, the yields from the multilayer and the crystal with equal thicknesses can be compared. The corresponding formula

$$\frac{N_{\lambda(\mathrm{cr})}^{\mathrm{PXR}}}{N_{\lambda(\mathrm{mul})}^{\mathrm{PXR}}} \approx \frac{\omega_{\mathbf{g}(\mathrm{cr})}^4}{\omega_{\mathbf{g}(\mathrm{mul})}^4}\frac{T_{(\mathrm{cr})}^3}{T_{(\mathrm{mul})}^3} \tag{30}$$

shows the higher yield of the multilayer as a PXR source using the above same arguments that were used concerning (23).

For completeness let us consider an influence of the interference between DTR and PXR on the total-emission properties. To calculate the interference term in the range of anomalous dispersion $|\tau(\omega)|<1$ one should take into account two branches of PXR waves in (12). Such a term is given by

$$\omega\frac{\mathrm{d}N_\lambda^{\mathrm{INT}}}{\mathrm{d}\omega\,\mathrm{d}^2\Theta} = \frac{2e^2}{\pi^2}\left\langle \frac{\Omega_\lambda^2}{\gamma^{-2}+\gamma_*^{-2}+\Omega^2}\left(\frac{1}{\gamma^{-2}+\Omega^2} - \frac{1}{\gamma^{-2}+\gamma_*^{-2}+\Omega^2}\right)\times\frac{\sinh^2(t_\lambda\sqrt{1-\tau_\lambda^2})}{\cosh^2(t_\lambda\sqrt{1-\tau_\lambda^2})-\tau_\lambda^2} \times\frac{(1-\sigma_\lambda\tau_\lambda)\sinh(t_\lambda\sqrt{1-\tau_\lambda^2})+\sigma_\lambda\sqrt{1-\tau_\lambda^2}\sin(t_\lambda(\sigma_\lambda-\tau_\lambda))}{\sigma_\lambda^2+1-2\sigma_\lambda\tau_\lambda}\right\rangle, \tag{31}$$

where $\sigma_\lambda = (\gamma^{-2}+\gamma_*^{-2}+\Omega^2)/|\chi_{\mathbf{g}}|\alpha_\lambda$. When this result is compared with that of (15), it is apparent that the ratio between the interference term and the DTR distribution can be estimated as $2(\gamma_*^2/\gamma^2)(1+\gamma_*^{-2}\Omega^2)$. This estimation shows that on the condition $\gamma \gg \gamma_*$, the contribution of interference term is small compared to DTR within the wide region of observation angles $\Theta \leqslant \gamma_*^{-1}$.

Analysis of the interference term outside the region of anomalous dispersion ($\tau_\lambda > 1$) shows that the contribution of this term is small compared to both PXR and DTR contributions as well. Obviously, the essential difference between PXR and DTR angular distributions for large electron energies $\gamma \gg \gamma_*$ is responsible for the small influence of this interference effect. Note, the case $\gamma < \gamma_*$ is of no interest because DTR contribution is negligible under these conditions.

2.4. *The emission from a thick absorbing target*

Now we consider X-ray emission from a thick absorbing target in order to estimate the maximum intensity from a multilayer structure. It should be noted that the influence of a photoabsorption on DTR and PXR properties is very different. Indeed, since DTR is due to the coherent scattering of fast-electron transition radiation, it is formed at the distance of the order of the extinction length $l_{\mathrm{ext}} \sim (\omega|\chi_{\mathbf{g}}|^{-1})$, which is usually smaller that the absorption length $l_{\mathrm{ab}} \sim (\omega\chi_0'')^{-1}$, $\chi_0'' = \frac{a}{T}\chi_a'' + \frac{b}{T}\chi_b''$. Therefore the influence of the photoabsorption on the DTR process is not of fundamental importance. To estimate such an influence let us now consider the general solution (12) for a semi-infinite absorbing target. Our analysis shows that the DTR spectral–angular distribution from an absorbing semi-infinite multilayer is described by the expression (15), where the quantity

$$R_\lambda^{\mathrm{DTR}} = \frac{1}{\left|\tau_\lambda - \mathrm{i}\beta_\lambda + \sqrt{\tau_\lambda - 1 - 2\mathrm{i}\beta_\lambda(\tau_\lambda-\kappa_\lambda)}\right|^2}, \tag{32a}$$

$$\beta_\lambda = \frac{\chi_0''}{|\chi_{\mathbf{g}}|\alpha_\lambda}, \qquad \kappa_\lambda = \frac{\sin\left(\pi\frac{a}{T}\right)}{\pi}\frac{\chi_a''-\chi_b''}{\chi_0''}\alpha_\lambda \tag{32b}$$

must be inserted as the reflection coefficient. The reflection coefficients R_λ^{DTR} from (32) and (15) for $t_\lambda > 1$ are close to each other, because the coefficient β_λ is usually much smaller than unity (β_λ is the ratio of the extinction length l_{ext} to absorption length l_{ab}).

On the other hand, since PXR is due to the scattering of a fast-electron equilibrium electromagnetic field, it is formed along the whole thickness of the target. Therefore the absorption determines PXR yield when l_{ab} is smaller than the target thickness. The PXR angular distribution, following from (12) and taking into account the photoabsorption in the limit $L \to \infty$, has the form

$$\frac{\mathrm{d}N_\lambda^{\mathrm{PXR}}}{\mathrm{d}^2\Theta} = \frac{2e^2\omega_{\mathrm{g}}^2\alpha_\lambda}{\pi g^2} t_{\lambda\mathrm{eff}} \times \left\langle \frac{\Omega_\lambda^2}{(\gamma^{-2}+\gamma_*^{-2}+\Omega^2)^2 - 2\kappa_\lambda(\gamma^{-2}+\gamma_*^{-2}+\Omega^2)|\chi_{\mathrm{g}}|\alpha_\lambda + |\chi_{\mathrm{g}}|^2\alpha_\lambda^2} \times \left(1 - \frac{|\chi_{\mathrm{g}}|^2\alpha_\lambda^2}{(\gamma^{-2}+\gamma_*^{-2}+\Omega^2)^2}\right)^2 \right\rangle, \tag{33a}$$

$$t_{\lambda\mathrm{eff}} = \frac{2\omega_{\mathrm{g}}^2\alpha_\lambda}{g^2} \frac{\sin^2\left(\frac{\varphi}{2}\right)}{\chi_0''}. \tag{33b}$$

When this result is compared with that of (26), it is apparent that the main change of PXR properties consists in the limitation on the value of effective thickness of the multilayer. A comparison of the quantity $t_{\lambda\mathrm{eff}}$ from (33b) and the definition (16) allows us to determine the optimum number of multilayer periods $M_{\mathrm{opt}}^{\mathrm{PXR}}$ for PXR generation

$$M_{\mathrm{opt}}^{\mathrm{PXR}} = \frac{\sin^2\left(\frac{\varphi}{2}\right)}{\pi\chi_0''} = \frac{\sin\left(\frac{\varphi}{2}\right)}{\omega_{\mathrm{B}}\chi_0''T} = \frac{l_{\mathrm{ab}}\sin\left(\frac{\varphi}{2}\right)}{T}. \tag{34}$$

It should be noted that the result (33) demonstrates the possibility of the effect of anomalous photoabsorption in PXR manifestation, which can be realized with the proviso that $\kappa_\lambda \approx 1$ and $(\omega_{\mathrm{g}}^2/\omega_{\mathrm{p}}^2)\alpha_\lambda \approx 1$, but these conditions call for the small ratio a/T, resulting in the decrease of the PXR yield proportional to $\sin^2(\pi\frac{a}{T})$.

3. Experimental results

The scheme of the experimental setup is shown in Fig. 3. The Tomsk Synchrotron has 20 ms beam

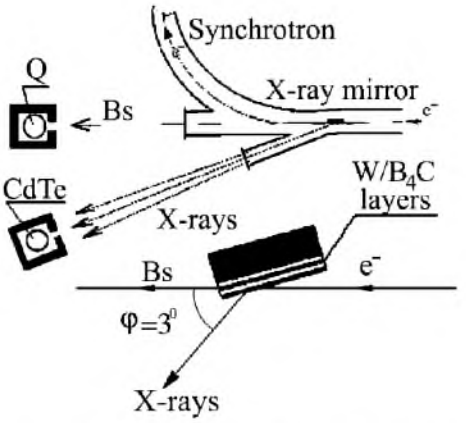

Fig. 3. The experimental setup: Q is γ-quantometer, CdTe is X-ray detector, X-mirror mounted on the goniometer head.

pulse with a 4 Hz repetition rate, resulting in a duty factor of 10%. Divergence of the 500-MeV electron beam was about 0.2 mrad. The multilayer was mounted in a goniometer and placed at the internal electron beam at the Bragg condition. The angle between the beam axis and the multilayer surface was about 1.5° at the symmetric position.

The multilayers used as the targets were created on a 380 μm Si plates by OSMIC Inc. as periodic structures consisted of the W and B_4C layers. The number of the layer pairs $M = 400$, the ratio of W and B_4C layer thickness are 0.33. The first multilayer had uniform spacing $T = 18$ Å, the second-cluster-graded spacing $T = 18.9$, 18.54, 17.56 and 17.14 Å (5 clusters, 80 periods each). The targets prepared from the multilayers for the experiment had the vertical and horizontal dimensions of 25 and 10 mm, respectively.

The photons generated in the multilayer were detected by a CdTe semiconductor detector placed at the angle $\varphi \simeq 3°$ with respect to the electron-beam direction at a distance of 440 cm from the target. The photon path in the air was about 262 cm. The detector aperture was 4 mm^2, the energy resolution at the ^{63}Zn line (8.1 keV) was about 10%. The bremsstrahlung γ-rays generated in the target were detected by γ-quantometer. Preliminary alignment of the targets was made with a laser. The final alignment was obtained by means

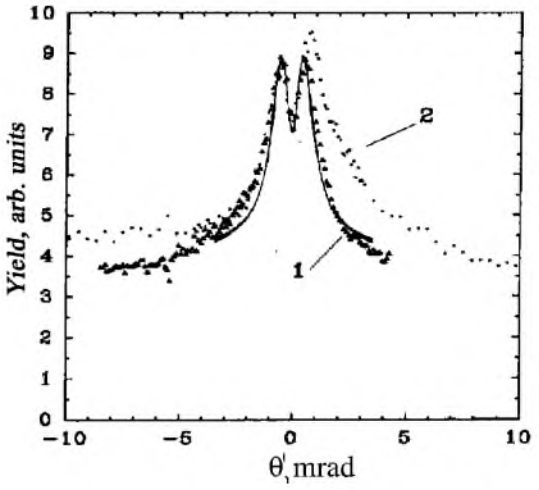

Fig. 4. The orientational dependencies (rocking curves) of the yield of 9.0–22.1 keV photons generated by the 500-MeV electron beam in the 400 WB_4C beleaguers the X-ray mirrors with uniform and cluster-graded spacing, curves 1, 2, respectively. Here the calculated rocking curve is presented as well.

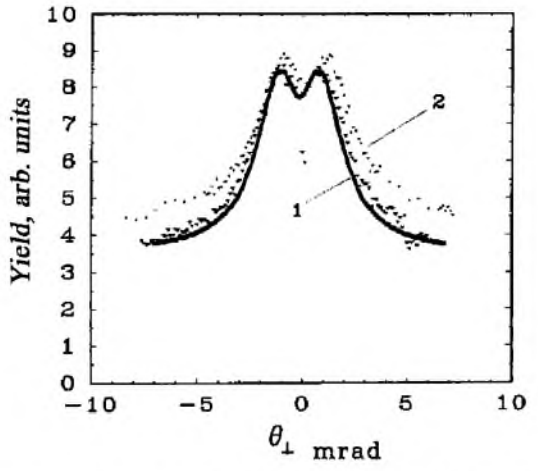

Fig. 5. The measured vertical cross-section of X-ray distributions emitted from X-mirrors with uniform and cluster-graded periods at the target orientation $\theta' = 0$, curves 1, 2, respectively. Calculated angular distribution and experimental data are normalized at one point.

of measuring the orientation dependence of the X-rays yield in the range of photon energy of 9–22.1 keV, which is near to the expected photon energy at the symmetric position of the multilayers.

Both the pulse-height spectra and the orientation dependence (rocking curve) of the photon yield in spectral peaks were measured. The vertical angular distributions of the yields were measured after aligning the targets in the symmetric position. The orientation dependencies from the uniform (curve 1) and cluster-graded (curve 2) multilayers normalized on the γ-quantometer current are given in Fig. 4. The vertical angular distribution from the uniform (curve 1) and cluster graded (curve 2) multilayers normalized in γ-quantometer current are given in Fig. 5. Both sets of curves show bright twin peaks with the intensity dips in the centers. The narrow minima at $\theta' = 0$ and $\Theta_\perp = 0$ appear when the target was exactly in symmetric position.

The spectra of radiation generated in the multilayer structures with uniform and cluster-graded periods obtained at the symmetrical target orientation are presented in Fig. 6; curves 1 and 2, respectively. As can be seen, the photon energy generated

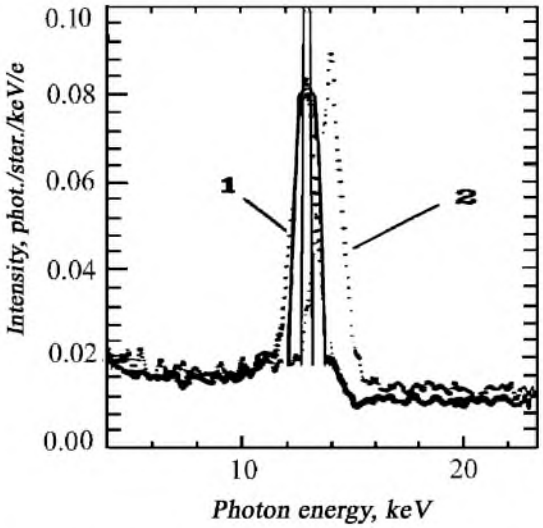

Fig. 6. The measured spectra 1, 2 of X-rays emitted for the target orientation $\theta' = 0$ corresponded to the uniform and cluster-graded period X-mirrors, respectively. Here the calculated spectrum is shown as well as such a spectrum averaged over detector energy resolution. The averaged spectrum and experimental data are normalized at one point.

in the cluster-graded multilayer is higher than that of the uniform multilayer.

4. Comparison with experimental results

Since the measurement of the current of the storage ring's electron beam was not available to us, the X-ray intensity was measured only in arbitrary units and the intensity enhancement in the multilayer structure in comparison to the crystal's could not be demonstrated. On the other hand, since the angular distributions or orientational dependencies of PXR and DTR are very different for the conditions of the experiment, we can determine the main emission mechanism.

To determine the relative contributions of DTR and PXR, we note that $\gamma_* \approx 273$ in accordance with (19) for our experimental parameters, so that the ratio $\gamma/\gamma_* \approx 3.66$. This value is not sufficient in order for DTR to determine the total yield of weakly collimated radiation, but it is quite sufficient for the separation of the contributions of DTR and PXR experimentally. Thus, the emission yield in our experiment was determined by both DTR and PXR contribution with X-rays concentrated in the vicinity of Bragg frequency $\omega_B \approx 13.4$ keV. Since the X-ray detector angular size $\Theta_d \approx 0.26$ mrad was smaller than the characteristic emission angle $\gamma^{-1} = 1$ mrad effectively determining the scale of the emission angular distribution, the spectral–angular density of emitted photons was measured. The number of periods sufficient for DTR yield formation $M_{\mathrm{opt}}^{\mathrm{DTR}} \simeq 188 < M = 400$ follows from (21). The angle of multiple scattering for electrons crossing such number of periods $\Psi_{\mathrm{sc}} \approx 1.06$ mrad exceeds essentially the initial beam divergence. Since the transition radiation is formed at a macroscopic distance on the order of the emission formation length (in our case this transition radiation is diffracted simultaneously by multilayer), the influence of the emitting electron's multiple scattering must be taken into account. In this work we took into account multiple scattering to calculate the DTR rocking curve and angular distribution in the vertical plane. It should be noted that the PXR angular maximum takes place in the vicinity of the angle $\Theta \approx \gamma_*^{-1} \gg \Psi_{\mathrm{sc}}$. Therefore the influence of multiple scattering on PXR angular distribution is not large in our experiment.

The orientation dependence of DTR, PXR and total-emission yield, calculated by the use of experimental parameters, is presented in Fig. 7. As can be seen, the expected angular density of X-rays generated in multilayers has the value 2 photons/electron·str.

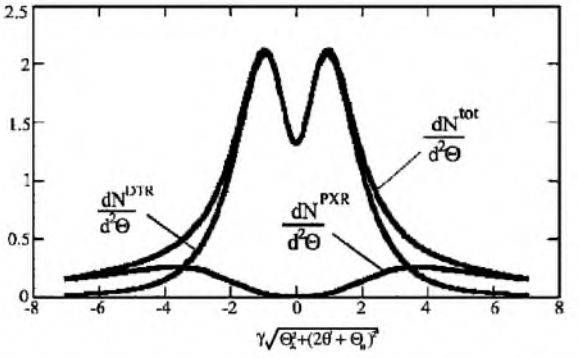

Fig. 7. The orientational dependence of PXR, DTR and total-emission yield, calculated by the use of experimental parameters; $x = \sqrt{\gamma^2\Theta_\perp^2 + \gamma^2(2\theta' + \Theta_{||})^2}$.

The calculated rocking curve and angular distribution of the total emission in vertical plane are presented in Figs. 4 and 5, respectively. Experimental data and theoretical curves are normalized in one point. As can be seen, theoretical and experimental results are in agreement.

To describe the spectrum of radiation from multilayer with uniform periods presented in Fig. 6, it is sufficient to use the formulae (15) and (24). These equations predict a very narrow spectrum of emitted radiation with the width $\Delta\omega \sim 100$ eV following (17). Since the energy resolution of the CdTe detector was about 10%, the measured spectrum differed from natural one. To compare theoretical and experimental results, the calculated spectrum was averaged over photon energies within the limits corresponding to detector energy resolution. The averaged spectrum and experimental data were normalized at one point. The averaged and non-averaged spectra calculated by the formulae (15) and (24) are presented in Fig. 6. As can be seen, calculated and measured spectra are in agreement.

As can be seen in Fig. 6, the energy of photons emitted from the multilayer with cluster-graded periods is larger than that of the case of uniform periods. This means that in the case of cluster-graded multilayer, the radiation is mainly

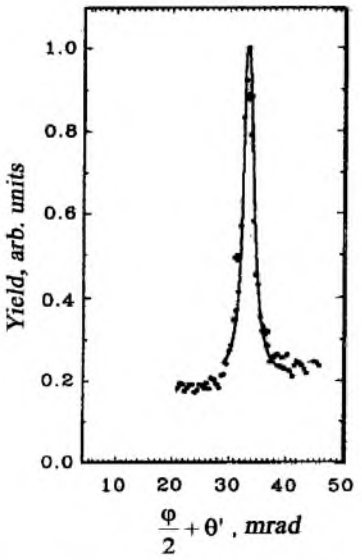

Fig. 8. A comparison of the calculated and measured [6] orientational dependence of the X-ray yield.

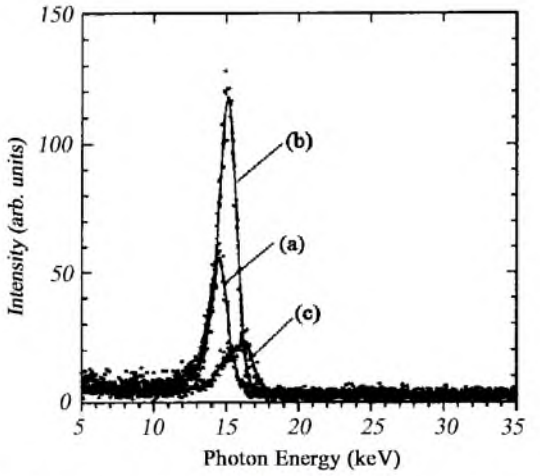

Fig. 9. The measured spectra [6]. $\Theta' = -0.117°$, 0°, 0.167° (curves a–c, respectively).

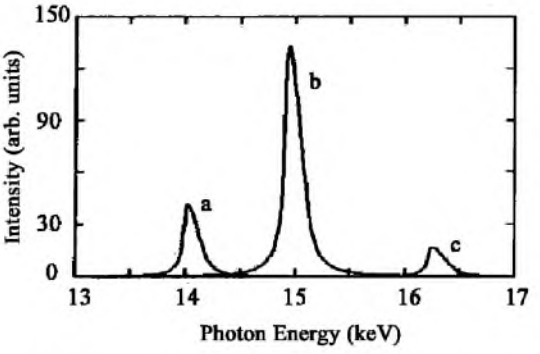

Fig. 10. The calculated spectra using experimental values of the orientational angle $\Theta' = -0.117°$, 0°, 0.167° (curves a–c, respectively). The shape, height and position of the peaks compares well with the measured in Fig. 9.

generated into the near-surface mirror-cluster having the smallest period, because the number of periods in a cluster $M_1 = 80$ is comparable with optimum value $M_{\text{opt}}^{\text{DTR}} \approx 120$.

Using our derived theory, an explanation of experimental results [6] is also given here. The measured orientational dependence of X-ray yield for this experiment is presented in Fig. 8. To estimate relative contributions of DTR and PXR, we compared the magnitudes of DTR and PXR angular distributions for the experimental parameters. We obtained the following estimations: $(dN^{\text{PXR}}/d^2\Theta)_{\max} \approx 6 \times 10^{-3}$ photons/electron·str. and $(dN^{\text{DTR}}/d^2\Theta)_{\max} \approx 0.8$ photons/electron·str. Thus DTR dominates in the measured emission yield. The theoretical orientational dependence is also presented in Fig. 8 (solid line). It was calculated without a PXR contribution and bremsstrahlung background. The PXR orientational dependence is much wider than that of DTR and cannot explain the experimental data. The calculated curve and experimental data are normalized at one point. As seen in the figure, the calculated curve agrees with data.

The spectra of collimated X-rays emitted from the multilayer structure placed at different angles relative to electron-beam direction were measured on the experiment [6] as well. The spectra of radiation generated in the multilayer, obtained for the orientational angles $\Theta' = -0.117°$, 0° and 0.167° are presented in Fig. 9. The emission spectra calculated by the use of experimental values of the orientation angle Θ' are presented in Fig. 10 (these spectra have been not averaged over the detector's energy resolution for better visualization of the natural spectral width of emitted photons). Comparing the experimental and calculated curves presented in Figs. 9 and 10, respectively, one can see

that the positions of emission peaks coincide. In addition, the relative amplitudes of the calculated peaks are close to those of the corresponding experimental peaks.

5. Conclusions

Our analysis has shown that PXR and DTR are the main emission mechanisms for relativistic electrons passing through a multilayer nanostructure. The relative contributions of these emission mechanisms to the total yield depend on the emitting electron's energy. If it is smaller than the critical energy $m\gamma_* = m\omega_B/\omega_p$, then PXR dominates. The PXR efficiency of a multilayer source can exceed that of a crystal. This occurs because of the larger number of multilayer electrons, which make a coherent contribution to the formation of X-ray emission yield. The number of emitted X-ray photons is about 10^{-4} per electron. Crystals are limited to 10^{-6}–10^{-5}.

If the energy of emitting electron exceeds the critical energy, then the PXR and DTR relative contributions depend on the ratio γ/γ_*, target thickness L, absorption length l_{ab} and the X-ray detector angular size Θ_d. The total yield can be determined by PXR contribution if $\Theta_d > \gamma_*^{-1}$ and the radiator is thick enough. On the other hand, DTR dominates if $\gamma \gg \gamma_*$ and $\Theta_d \leqslant \gamma^{-1}$. The efficiency of the DTR source is approximately the same as that of PXR radiator: 10^{-4} photons per electron, but the important advantage of DTR consists in having a larger angular photon-density value.

Our theory has been compared with our experimental results and we have shown that the observed X-ray yield is explained by DTR. The obtained theoretical and experimental results demonstrate the possibility of making an X-ray source intense enough for medical and other applications [30,31]. The analytical impressions derived in this work allow one to calculate most of the needed characteristics of such a source.

The brightness and efficiency of the source can be improved further by using a cyclical accelerator wherein the electron beam is passed through a multilayer many times. In this scheme, a thin multilayer would be installed inside the vacuum chamber of a cyclical accelerator such as a betatron. Multipassing of the electron beam through thin targets has been demonstrated experimentally [32].

Acknowledgements

This work was supported by the United States National Institute for Health under Small Business Innovation Research (SBIR) program (Grant No. 2-R33CA086545-02) and by the Russian Foundation of Basic Research (Grant No. 03-02-96431).

References

[1] V.L. Ginzburg, I.M. Frank, J. Phys. (Moscow) 9 (1945) 3533.
[2] M.A. Kumakhov, Phys. Lett. A 5 (1976) 17.
[3] V.G. Baryshevsky, I.D. Feranchuk, Zh. Eksp. Teor. Fiz. 61 (1971) 944.
[4] G.M. Garibian, S. Yang, Zh. Exp. Teor. Fiz. 61 (1971) 930.
[5] R. Carr, Nucl. Instr. and Meth. B 122 (1994) 625.
[6] V.V. Kaplin, S.R. Uglov, V.N. Zabaev, M.A. Piestrup, C.K. Gary, N.N. Nasonov, M.K. Fuller, Appl. Phys. Lett. 76 (2000) 3647.
[7] N.N. Nasonov, V.V. Kaplin, S.R. Uglov, M.A. Piestrup, C.K. Gary, Phys. Rev. E 68 (2003) 36504.
[8] M.L. Ter-Mikaelian, High Energy Electromagnetic Processes in Condensed Media, Wiley, New-York, 1972.
[9] M.L. Cherry, D. Muller, T.A. Prince, Nucl. Instr. and Meth. 115 (1974) 141.
[10] M.J. Moran, B.A. Dahling, P.J. Ebert, M.A. Piestrup, B.L. Berman, J.O. Kerhart, Phys. Rev. Lett. 57 (1986) 1223.
[11] M.A. Piestrup, D.G. Boyers, C.I. Pincus, Q. Li, G.D. Hallwell, M.J. Moran, X.K. Maruyama, D.D. Snyder, R.M. Silzer, D.M. Skopik, G.B. Rothbart, Phys. Rev. A 45 (1992) 1183.
[12] V.G. Baryshevskiy, I.D. Feranchuk, J. Phys. (Paris) 44 (1983) 913.
[13] A. Caticha, Phys. Rev. A 40 (1989) 4322.
[14] Yu.N. Adishchev, S.A. Vorob'ev, B.N. Kalinin, S. Pak, A.P. Potylitsin, Sov. Rhys. JETP 63 (1986) 484.
[15] A.V. Shchagin, V.I. Pristupa, N.A. Khithnyak, Phys. Lett. A 148 (1990) 485.
[16] K.H. Brenzinger, C. Herberg, B. Limburg, H. Backe, S. Dambach, H. Euteneuer, F. Hagenbuck, H. Hartmann, W. Schope, Th. Walcher, Zh. Rhys. A 358 (1997) 107.

[17] N. Zhevago, in: Proc. II Symp. on Transition Radiation of High Energy Particles, Yerevan, Armenia, 1983, p. 200.
[18] C.T. Law, A.E. Kaplan, Opt. Lett. 12 (1987) 900.
[19] B. Pardo, J.M. Andre, Phys. Rev. A 40 (1989) 1918.
[20] M.S. Dubovikov, Phys. Rev. A 50 (1994) 2068.
[21] J.M. Andre, B. Pardo, C. Bonnelle, Phys. Rev. E 60 (1999) 968.
[22] B. Lastdrager, A. Tip, J. Verhoeven, Phys. Rev. E 61 (2000) 5767.
[23] B. Pardo, J.M. Andre, Phys. Rev. E 65 (2002).
[24] N.K. Zhevago, V.I. Glebov, Phys. Lett. A 309 (2003) 311.
[25] Z.G. Pinsker, Dynamic Scattering of X-rays in Crystals, Springer, Berlin, 1981.
[26] I.D. Feranchuk, A.V. Ivashin, J. Phys. (Paris) 46 (1985) 1981.
[27] X. Artru, P. Rullhusen, Nucl. Instr. and Meth. B 145 (1998) 1.
[28] N. Nasonov, in: H. Wiedermann (Ed.), Electron–Photon Interaction in Dense Media, Kluwer Academic Publisher, 2002, p. 49.
[29] A.M. Afanasyev, M.A. Aginian, Zh. Exp. Teor. Fiz. 74 (1978) 570.
[30] M.A. Piestrup, X. Wu, V.V. Kaplin, S.R. Uglov, J.T. Cremer, D.W. Rule, R.B. Frioito, Rev. Sci. Instr. 72 (2001) 2159.
[31] C.K. Gary, M.A. Piestrup, D.G. Boyers, C.I. Pincus, R.H. Pantell, G.B. Rothbart, Med. Phys. 204 (1993) 1527.
[32] V.V. Kaplin, S.R. Uglov, O.F. Bulaev, V.J. Goncharov, M.A. Piestrup, C.K. Gary, Nucl. Instr. and Meth. B 173 (2001) 3.